Control growth of PbS quantum dots doped sono-ormosil

R. Erce-Montilla
Dpto. Física de la Materia Condensada, Universidad de Cádiz, Aptdo. 40, 11510 Puerto, Real (Cadiz), Spain

M. Piñero
Dpto. Física Aplicado, Univeridad de Cádiz, Aptdo. 40, 11510 Puerto, Real (Cadiz), Spain

N. de la Rosa-Fox and A. Santos
Dpto. Cristalografía y Mineralogía, Estratigrafía, Geodinámica y Petrología y Geoquímica, Universidad de Cádiz, Aptdo. 40, 11510 Puerto, Real (Cadiz), Spain

L. Esquivias
Dpto. Física de la Materia Condensada, Universidad de Cádiz, Aptdo. 40, 11510 Puerto, Real (Cadiz), Spain

(Received 31 December 2000; accepted 21 June 2001)

Semiconductor PbS quantum dots doped-SiO_2 organically modified silicate (ormosil) gels were synthesised via sol-gel by using high-power ultrasounds (sonogel). The effect of PbS crystal concentration and the addition of (3-mercaptopropyl)trimethoxysilane acting as surface capping agent (SCA) were investigated. By adjustment of the SCA to lead ratio, PbS nanoparticles of different sizes and morphologies were obtained. Textural parameters were calculated from N_2 physisorption isotherms. The PbS galena phase was identified by x-ray diffraction, the crystal size by high-resolution transmission electron microscopy, and the exciton confinement by ultraviolet–visible–near-infrared spectrophotometry. Crystallite mean sizes of spheres and cubes ranging from 6.5 to 10.5 nm and needles 7-nm wide and 15–20 nm long, for different PbS and SCA concentrations, were obtained. These results differ from those predicted by the effective mass approximation corroborating the band gap modifications in the smallest nanocrystals. The method allows the control of the crystal size and improves the stabilization of the PbS nanocrystals.

I. INTRODUCTION

Electronic and optical properties of IV–VI semiconductors have been the object of extensive research in the last three decades. Their narrow band gap permits the creation of a strongly quantum confined exciton (one electron–hole pair) when microcrystallites are smaller than the bulk exciton Bohr radius (a_B = 18 nm for the PbS) (quantum dots).[1–3] This is the case for PbS crystallites presenting a particle size smaller than 18 nm, with a threshold of absorption of 0.41 eV for the bulk material. Many approaches have been explored for the preparation of small PbS clusters and its incorporation into solid and transparent matrices.[4–6] One of them is the use of the sol-gel process combined with colloidal chemistry.[7–9] This technique avoids agglomeration permitting the control of particle size and size distribution but produces instability of the small precipitates. However, surface-capping methods[10] may help to overcome the last drawback.

Gel matrices and films have been used as hosts for semiconductor quantum dots from more than 10 years, mainly because low temperatures are required to create the network. On the other hand, they present a high porosity that makes them especially active for humid condensation and oxidation, thus favoring subsequent crystal growth. In spite of these inconveniences, this issue arouses interest and recently several works have been reported.[11] Sealing pores and reducing the specific surface area could reduce the oxidation. One of the methods to achieve this is by using organic polymers in the gel formation, which allow the synthesis of mechanically improved silica gel matrices via copolymerization with silicon precursors, named ormosils. These hybrid organic–inorganic resulting materials present properties that make them especially attractive for optical requirements.[16,17]

The sol-gel method also offers variable and flexible processing conditions for developing workable optical devices. Thus, for example, the use of high-power

ultrasound radiation in the early steps of the process has proven to be an excellent tool for controlling the texture and pore size radii of the final material.[18] This method avoids the presence of an alcoholic common solvent, which is needed to obtain an alkoxide-water homogeneous mixture. Besides this, textural parameters are very sensitive to the supplied sonic power, as well as gelation temperature and sol pH.[19,20]

Solventless gels and ormosils prepared by sonocatalysis exhibit suitably features to incorporate and provide control uniform size of quantum dots. Among others, shorter gelation times, higher matrix densities, smaller pore radii, and narrower pore-size distribution result compared to those obtained from classic gels.[21,22] As a consequence, thermal and mechanical stability of the resulting sonogels and sono-ormosils are improved in relation with other kind of gels[23,24] used as host matrices for supporting dispersed semiconductor nanoparticles.

We present in this paper the synthesis of PbS quantum dots stabilized with surface-capping agents (SCA), incorporated into rigid transparent SiO_2 sono-ormosils for nonlinear optical applications.

II. EXPERIMENTAL

The chemical route for the preparation of the host gel is schematized in Fig. 1 and described as follows: Tetramethyl forthosilicate, $Si(OMe)_4$ (TMOS), was first partially hydrolyzed with HNO_3 catalyst in a molar ratio of $TMOS:H_2O:HNO_3$ of 1:0.84:0.026. Organic polymer poly(dimethyldisiloxane) (PDMS) was added in a molar ratio TMOS:DMS of 0.19, where the organic fraction in the hybrid material has been expressed as a function of the methyldisiloxane monomer, DMS. The resulting solution (sol A) was submitted to 320 J cm^{-3} ultrasound energy, and then it was poured and kept in hermetically closed containers at 50 °C for 24 h.

In sol A, the hydrolysis was completed by adding nitric acid water with a molar ratio $TMOS:H_2O:HNO_3$ of 1:3.36:0.0015 to complete the water stoichiometry. The nucleation of PbS was promoted by adding suitable amounts of lead acetate and MPTMS, to test the influence of the SCA on the further control growth of the colloidal particles of PbS. Table I summarizes the molar ratio used in the outlined samples. The code sample is referred as *XRY*, *X* being the nominal PbS wt% and *Y* the MPTMS/Pb molar ratio. Finally thioacetamide (TAA) was added into the matrix solution to obtain the respective PbS wt%.

As shown in Fig. 1, lead and sulfur ions were added separately as two different solutions of lead acetate and TAA, both in 0.5 ml of methanol which supposes 0.74 mol of MeOH/mol of TMOS. At this step, the resulting solution (sol B) received 500 J/cm^{-3} of ultrasound energy. As in acidic medium PbS precipitation is

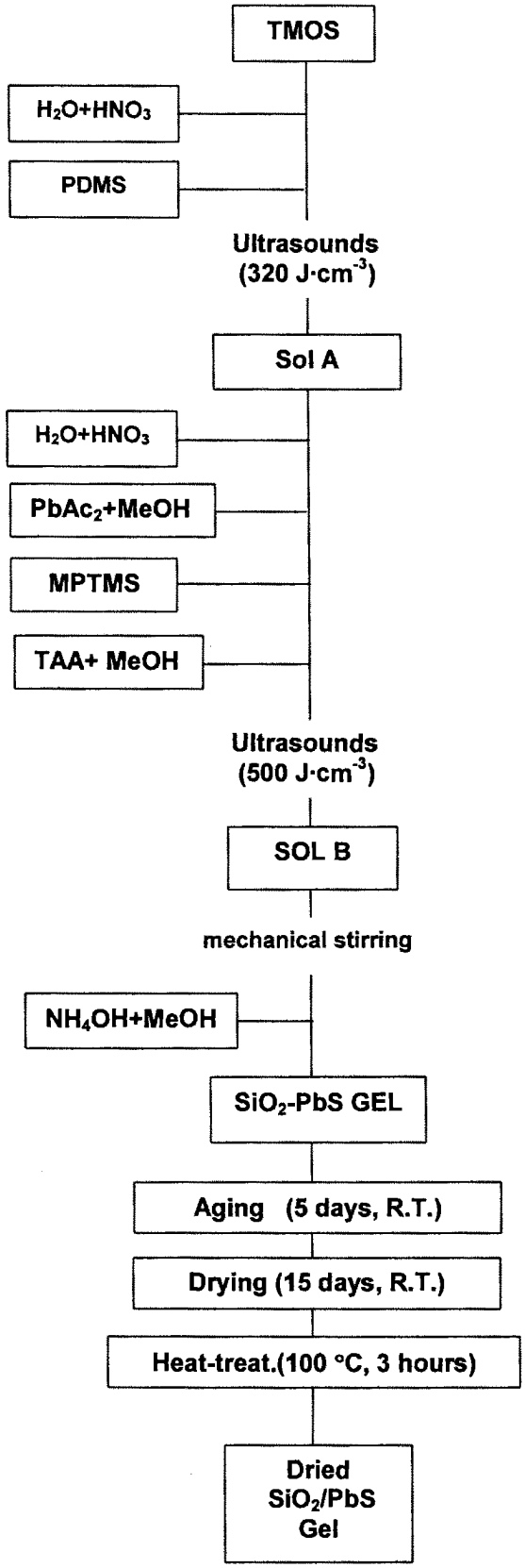

FIG. 1. Schematic experimental route for preparing PbS–SiO_2 composites by the sonocatalytic method.

TABLE I. Molar ratios respect to TMOS of the reactive precursors used in the preparation of PbS ormosils. The PDMS was added in a 10% volume ratio to TMOS volume in the four samples signaled.

Sample	$PbAc_2$	MPTMS ($\times 10^{-3}$)	TAA
0.5R32	1.35	41.6	1.8
1R10	2.7	26.0	3.6
4R5	10.8	52.0	14.

favored, we proceeded to increase the sol pH by addition of an ammonium hydroxide (NH_4OH) methanolic solution under mechanical stirring. The molar ratios of NH_4OH:TMOS varied from 0.04 to 0.06, and at this step the MeOH:TMOS molar ratio was 2.22. Then the total molar ratio MeOH:TMOS was 3.68 for both the PbS-doped samples and the undoped matrix, in order to use the same dilution rate.

The sol B was then poured into plastic containers, and gelation took place between 10 and 60 min. Following Fig. 1, the gel was aged at room temperature during 5 days closed airtight, to strengthen, and subsequently dried slowly for another 15 days by putting several holes on the cover. Samples were heat-treated up to 100 °C at 1 °C/min for 3 h in N_2 atmosphere.

Thermogravimetric analyses were performed at 10 °C/min up to 900 °C (Setaram Setsys 16/18). Textural parameters of gels were calculated by N_2 physisorption isotherms at 77 K using a Sorptomatic 1990 from Fisons. Specific surface area was calculated by the Brunauer–Emmett–Teller analysis (BET)[25] equation, and pore size distribution, by the Horvath–Kawazoe[26] method in the absorption branch. Prior to the measurements the powder samples were outgased at 100 °C.

The crystalline phases of the nanocrystals were identified by x-ray diffraction (XRD) using a Philips (PW 1710, 40 kW) diffractometer. The intensities were measured at room temperature with the Cu Kα line and a graphite monochromator in the diffracted beam. Data were collected over the 2θ range 20° to 80° at intervals of 0.04° at a step counting time of 10 s.

Optical absorption measurements were carried out on polished samples 1-mm thick, by using an ultraviolet–visible–near-infrared Perkin-Elmer Lambda19 spectrophotometer ranging from 300 to 1200 nm of wavelength. The crystal size and size distribution were calculated by a high-resolution transmission electron microscope (HRTEM, JEOL-2000). Electron diffraction on selected area for some crystals gave us information about the PbS crystalline phase.

III. RESULTS AND DISCUSSION

Visually, the gradation from yellow to dark red color of the as-prepared doped samples contrasts with the transparency of the undoped matrix, revealing the formation of PbS crystals. The thermograms performed on both undoped matrix and the 0.5R32 sample (Fig. 2) show a first weight loss at 120 °C due to the removal of residual adsorbed water and alcohol trapped into the porosity of the gels. Carbonized residues due to the polymer decomposition, taking place in the step at 180 °C, turned dark both samples. This result allowed us to optimize the heat treatment of the samples. A third weight loss at 230 °C could be assigned to the oxidation from the other organic precursors. The weight loss at 420 °C, which only appears in the doped sample, must be attributed to PbS decomposition, resulting in a colorless doped sample. Finally, a small weight loss at 475 °C corresponds to the water expelling as a byproduct of polycondensation of the remaining hydroxyl groups.

N_2 physisorption isotherms of the undoped matrix, 0.5R32 and 4R5 samples, are shown in Fig. 3. All of the curves show the typical features of a type I isotherm, characterized by a knee at low relative pressure ($P/P_0 < 0.2$) and a horizontal plateau in almost the whole relative pressure range with a sharp increase near saturation pressure. No hysteresis loop is noticeable; this is the typical signature of microporous solids by the absence of capillary condensation in mesopores. For the 0.5R32 sample (top curve) it is apparent the existence of an open structure, probably due to the steric effects coming from the SCA molecules. In the other side, the 4R5 sample (bottom curve) exhibits a closed structure as the result of a combination of both a low SCA content with lower steric influence and a high PbS content which in part may fill up the pores.

Table II shows the textural parameters evaluated from N_2 isotherms. A decrease in the specific surface area with an increase in the PbS content is observed. The correlation coefficients correspond to the linear regression of the BET equation. We consider that this behavior could be due to some differences in pore sizes as a consequence of the steric effects coming from the nonbonded 3-mercaptopropyl groups, since they are electrostatically opposite to the silica network. This assumption is confirmed by the good agreement existing between the apparent densities calculated from the porous volume and from the geometrical dimensions. Bulk density (ρ_s) was evaluated by taking into account the corresponding weight percent in the composite $(SiO_2)_{1-x}$–$(PbS)_x$ by using 2.2 g cm^{-3} for vitreous silica and 7.5 g cm^{-3} for PbS. Finally, average pore sizes in the last column corroborate the fine porosity of the host matrix.

To identify the crystalline phase of the particles embedded in the matrix, we proceed to remove the solvent from the ormosil-stabilized doped sols, by heat treatment at 50 °C prior gelation. The XRD pattern of the resulting precipitate was registered and compared with that of the amorphous matrix and then subtracted, resulting in the well-known galena pattern, as can be seen in Fig. 4.

HRTEM and electron diffraction on the selected area corroborated the above results. Figure 5(a) reports a HRTEM micrograph corresponding to the 0.5R32 sample, where it can be observed the distribution of spherical PbS nanocrystals, surrounded by the amorphous gel matrix. The crystalline structure was confirmed by electron diffraction analysis, as it is shown by the corresponding pattern included on the inset in Fig. 5(b). From the micrograph, the particle diameter and its distribution were calculated [Fig. 5 (b)], giving a mean value of 6.5 nm with a standard deviation of 0.9. In the same way, the HRTEM micrograph from the 1R10 sample is shown in Fig. 6(a). Spherical and/or cubic particles morphology and lattice planes in some cases can be clearly noticed. A mean diameter of around 10.5 nm with a standard deviation of 1.2 nm was obtained from the distribution plotted in Fig. 5(b). This range of crystal size suggests that PbS nucleates prior to gelling process and its further growth is controlled by the SCA. After the gel formation and during the consolidation of the silica network surrounding the PbS crystals, the subsequent aggregation and precipitation of them are hindered, giving the stabilization of the PbS crystal size.

On the other hand, neither spherical nor cubic PbS particles were observed by HRTEM in the higher PbS content 4R5 sample. In this case, we detected the formation of PbS particles maintaining the galena crystallographic structure but presenting a needle morphology, with mean size of 7-nm wide and 15–20-nm long, as it is shown in Fig. 7(a). This kind of morphology has been previously reported by other authors[27,28] and related with the early stages of the nanocrystal formation when colloidal techniques are involved for synthesizing PbS. The formation of this particle morphology in this sample must be due to its relatively low MPTMS:Pb molar ratio and the high PbS content. Then, the capping action

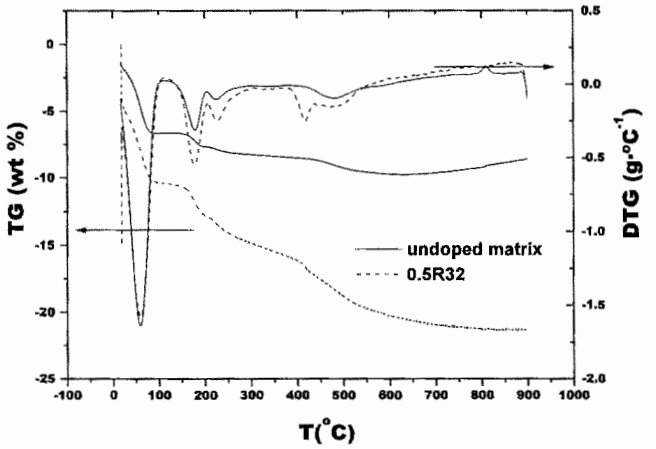

FIG. 2. TG weight loss curves for both the 0.5R32 and the undoped matrix samples. Derivatives of TG are included to emphasize the onset of the different weight losses.

TABLE II. Specific surface area (S), Pore volume (V_p), and apparent density (ρ_a) calculated from N_2 physisorption data. The apparent density (ρ) is evaluated from geometrical measurement, and the pore size, from cylindrical pores.

Sample	S (corr. coeff.) ($m^2\ g^{-1}$)	V_p ($cm^{-3}\ g^{-1}$)	ρ_a[a] ($g \cdot cm^{-3}$)	ρ[b] geometric ($g\ cm^{-3}$)	Pore size (nm)
Undoped matrix	616 (0.9994)	0.324	1.28	1.29 ± 0.05	2.10
0.5R32	677 (0.9989)	0.483	1.07	1.03 ± 0.05	2.86
1R10	542 (0.9990)	0.468	1.09	1.08 ± 0.05	3.46
4R5	414 (0.9978)	0.210	1.56	1.55 ± 0.05	2.02

[a] $1/\rho_a = V_p + 1/\rho_s$.
[b] Parallelopiped casting.

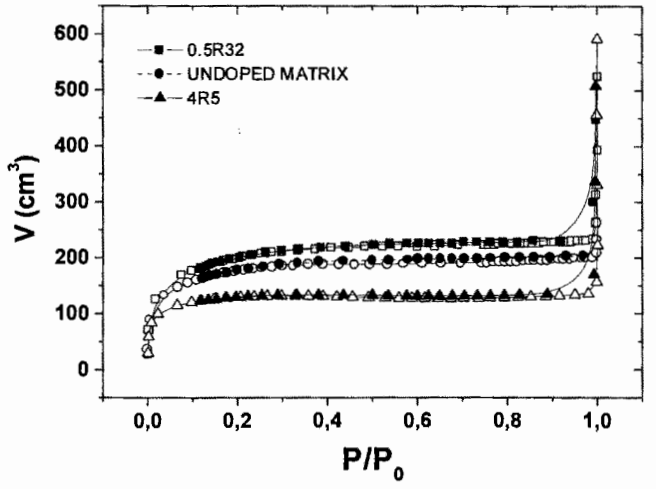

FIG. 3. N_2 physisorption isotherms of the 0.5R32, undoped matrix, and 4R5 samples. Solid and open symbols correspond to the adsorption and desorption branch, respectively.

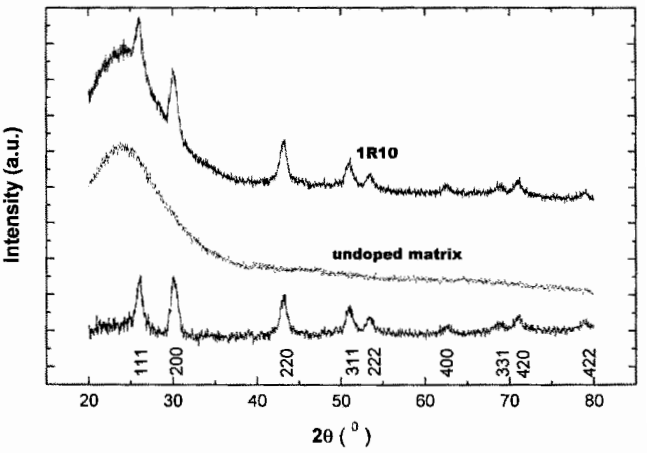

FIG. 4. XRD spectra of 1R10 powder sample dried at 50 °C and from the undoped ormosil matrix. The resulting diagram placed at the bottom was obtained from the corresponding subtraction between the outlined patterns and corresponds to galena PbS crystal.

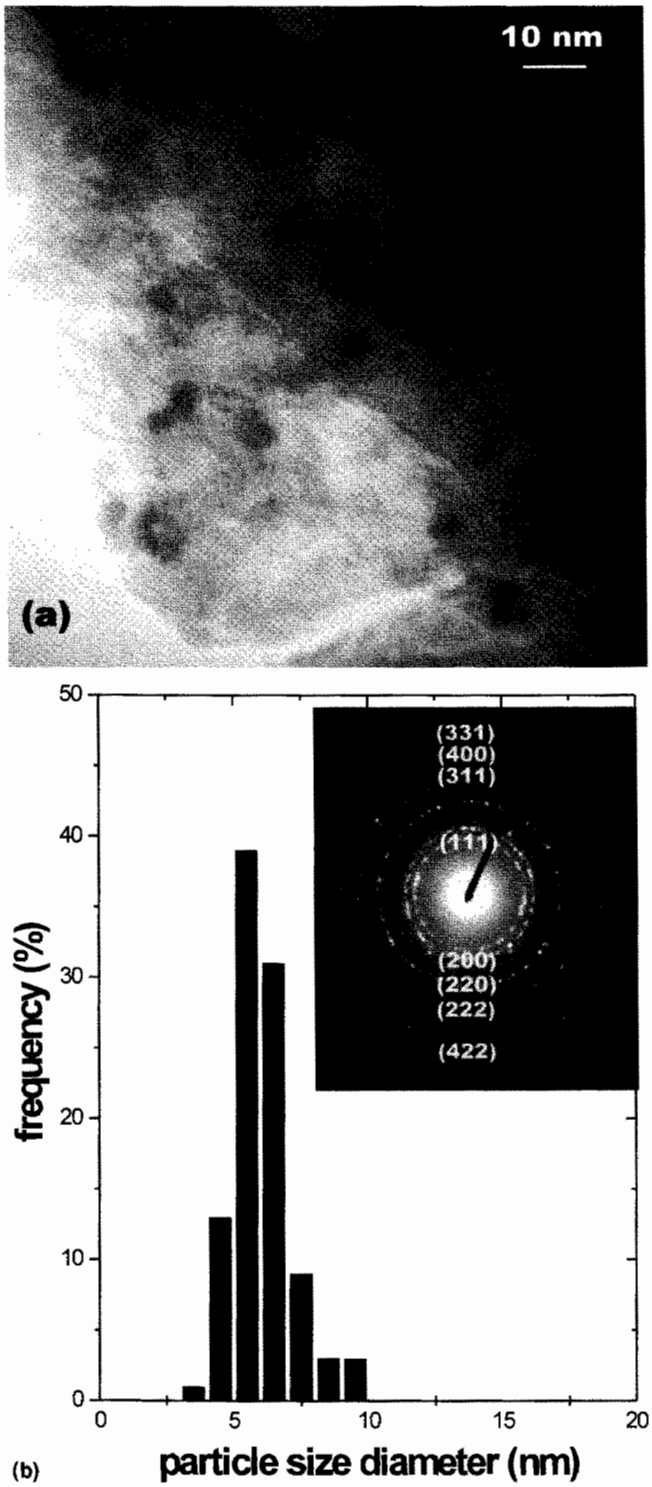

FIG. 5. (a) HRTEM micrograph of PbS nanoparticles of the 0.5R32 sample. (b) Particle size diameter distribution and, in the inset, the electron diffraction pattern with the corresponding values of interplanar spacing.

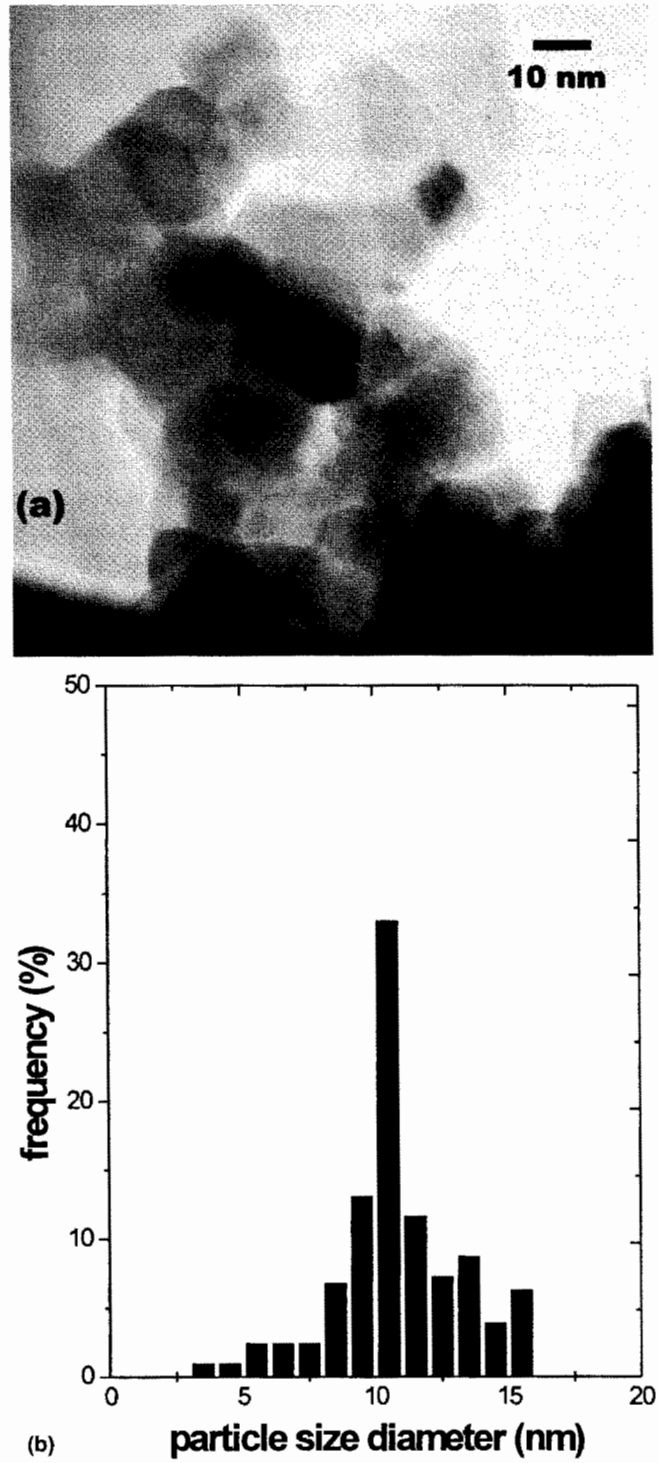

FIG. 6. (a) HRTEM and (b) particle size diameter distribution from the 1R10 sample.

cannot be as effective as in the other samples with higher MPTMS:Pb molar ratios. This could explain the preferred particle growth of PbS in the [200]-direction leading to the observed needle morphology [Fig. 7(b)].

The optical absorption spectra of the samples are depicted in Fig. 8; to allow comparison the transparent undoped matrix is included (bottom curve). All of the doped samples show a strong blue-shift of the absorption band from bulk PbS at 0.41 eV. This result reveals the opening of the band gap due to the small-sized

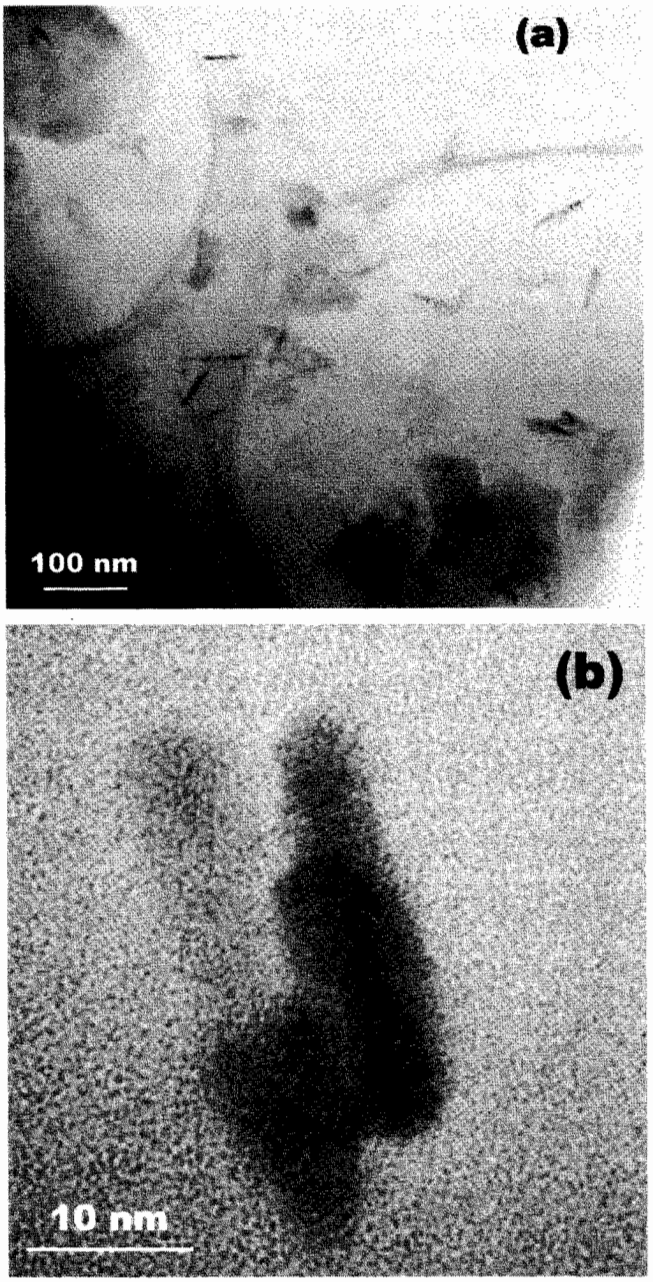

FIG. 7. (a) HRTEM from the 4R5 sample showing the needle morphology of PbS and (b) magnification from picture (a).

nanocrystals. It is well known, according to the EMA model,[29] that the first allowed excited state in quantum dots splits from the bulk band gap as $1/R^2$ and depends on the exciton reduced effective mass, $0.085m_e$ for bulk PbS, m_e being the electron rest mass. The influence of the Coulombic and polarization terms can be neglected due to the large dielectric constant ($\epsilon_\infty = 17$) and the ionic character of the PbS. Since the creation of an exciton responsible for the band gap involves the transfer of an electron from an S to a Pb atom, resulting in a rearrangement of ionic charge, then no new separation of charges take place.

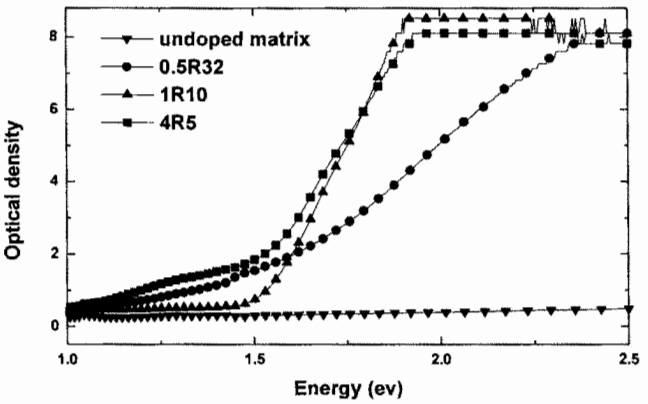

FIG. 8. Optical absorption spectra of the 0.5R32, 1R10, and 4R5 samples. The undoped matrix absorption curve, has been also included to show its transparency in all spectral ranges where samples behave its band gap.

Then, the blue-shift of the optical absorption band can be assigned to the quantum confinement of the exciton in PbS nanocrystals. However, some features can be appreciated in Fig. 8. First the long tail shown by the 05R32 sample is due to the high SCA content instead of a wide size distribution, in line with its size distribution [Fig. 5(b)], as a consequence of the excess of sulfur ions on the PbS crystal surface, coming from the SCA molecules, which act as hole traps generating lower energy states. Second and contrarily, the tail shown by the 4R5 sample is due to the needle morphology and the absorption curve presents a shoulder centered around 1.31 eV. Such a decrease in energy (240 meV) from the absorption band accounts for a weaker exciton confinement along the needle since in the direction of the needle the size (20 nm) is comparable with the PbS exciton Bohr radius (18 nm). For the other sample 1R10, in Fig. 8, one cannot discern the above mentioned effects.

As reported by other authors,[30,32] the nonresolved subbanding accounts for the trap states on the crystal surface, the particle size distribution, and/or indirect transition due to the quantized single particle states. This behavior is clearly identified on the optical spectra in Fig. 9, where the PbS content is maintained constant (0.5 wt%) and the SCA:PbS molar ratio varies from 5 to 64. As can be seen, the band gap shifts to higher energies as the SCA content increases. This result must be accompanied with a decrease in crystal size, implying a stronger quantum confinement effect. On the other hand, the appearance of the long tail in the lower energy side is noticeable for higher SCA content ($R > 20$) as it was seen in Fig. 8, thus corroborating our hypothesis.

At this point, one of the consequences of these interface-related trap states provoked by the nonbonded SCA molecules is an overestimate of the crystal size with respect to the EMA model. This fact suggests either a deep

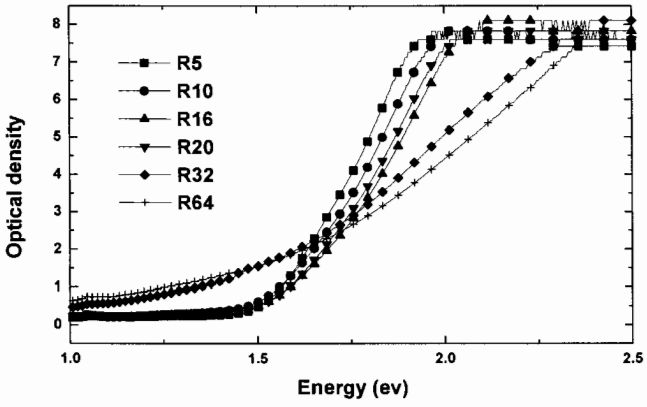

FIG. 9. Optical absorption spectra of the influence of the MPTMS: PbS molar ratio on band-gap shift in samples with a fix 0.5 wt% PbS content.

modification of the quantum dot electronic structure or a biexciton (two electron-hole pairs) formation in the smallest nanocrystals ($R < a_B$).

IV. CONCLUSIONS

Sono-ormosils prepared by the sol-gel route are especially attractive to act as a host matrix to support extremely fine dispersions of semiconductor crystals such as PbS. The method allows a homogeneous dispersion of PbS crystals embedded in the microporous silica matrix stabilized at 100 °C (2-nm average pore size). Steric effects of the SCA molecules affect the textural parameters. Uniform particle size is controlled by the action of the SCA. The range of PbS nanocrystal sizes suggests that they are nucleated prior to the gel formation. The blue-shift of the optical absorption band reveals the existence of quantum confinement effects of the nanocrystals. High SCA content provokes the absence of subbanding as well as the long tail in absorption curves due to the interface-related trap processes.

ACKNOWLEDGMENTS

This work has been supported by the Spanish CICyT under the Project MAT98-0798 and by the Plan Andaluz de Investigacion (TEP-0115).

REFERENCES

1. U. Woggon, in Optical Properties of Semiconductors Quantum Dots (Springer-Verlag, STMP Vol. 136, Berlin, Germany, 1997), Chap. 1 and 2.
2. N. Peyghambarian, S. Koch, and A. Mysyrowicz, in *Introduction to Semiconductor Optics* (Prentice-Hall, Upper Saddle River, NJ, 1993), pp. 245–253.
3. A. Lipovskii, E. Kolobkova, V. Petrikov, I. Kang, A. Olkhovets, T. Krauss, M. Thomas, J. Silcox, F. Wise, Q. Shen, and S. Kycia, Appl. Phys. Lett. **71,** 3406 (1997).
4. N.F. Borrelli and D.W. Smith, J. Non-Cryst. Solids **180,** 25 (1994).
5. M. Mukherjee, A. Datta, and D. Chakravorty, J. Mater. Res. **12,** 2507 (1997).
6. F. del Monte, Y. Xu, and J.D. Mckenzie, J. Sol-Gel Sci. Technol. **17,** 37 (2000).
7. S. Gallardo, M. Gutiérrez, A. Henglein, and E. Janata, Ber. Bunsen-Ges. Phys. Chem. **93,** 1080 (1989).
8. M. Guglielmi, A. Martucci, J. Fick, and G. Vitrant, J. Sol-Gel Sci. Technol. **11,** 229 (1998).
9. A. Martucci, P. Innocenzi, J. Fick, and J.D. Mackenzie, J. Non-Cryst. Solids **244,** 55 (1999).
10. L. Spanhel, E. Arpac, and H. Schmidt, J. Non-Cryst. Sol. **147&148,** 657 (1992).
11. N.N. Parvathy, G.M. Pajonk, and A. Venkateswara, J. Cryst. Growth **179,** 249 (1997).
12. N.N. Parvathy, G.M. Pajonk, and A. Venkateswara, Mat. Res. Bull., **32,** 397 (1997).
13. A. Martucci, M. Guglielmi, and K. Urabe, J. Sol-Gel. Sci. Technol. **11,** 105 (1998).
14. A. Martucci, J. Fick, J. Scell, G. Battaglin, and M. Guglielmi, J. Appl. Phys. **86,** 79 (1999).
15. M. Guglielmi, A. Martucci, E. Menegazzo, G.C. Righini, S. Pelli, J. Fick, and G. Vitrant, J. Sol-Gel Sci. Technol. **8,** 1017 (1997).
16. H. Lin, E. Bescher, J.D. Mackenzie, H. Dai, and O.M. Stafsudd, J. Mater. Sci. **27,** 5523 (1992).
17. P.T. Guerreiro, S. Ten, N.F. Borrelli, J. Butty, G.E. Jabbour, and N. Peyghambariam, Appl. Phys. Lett. **71,** 1595 (1997).
18. N. del Rosa-Fox, L. Esquivias, and J. Zarzycki, J. Mater. Sci. Lett. **10,** 1237 (1991).
19. N. del Rosa-Fox, L. Esquivias, A.F. Craievich, and J. Zarzycki, J. Non-Cryst. Solids **121,** 211 (1990).
20. E. Blanco, L. Esquivias, R. Litran, M. Piñero, M. Ramirez-del-Solar, and N. de la Rosa-Fox, Appl. Organomet. Chem. **13,** 399 (1999).
21. K. Morita, Y. Hu, and J.D. Mackenzie, in *Better Ceramics Through Chemistry V,* edited by M.J. Hampden-Smith, W.G. Kemplerer, and C.J. Brinker (Mater. Res. Soc. Symp. Proc. **271,** Pittsburgh, PA (1992), p. 693.
22. N. de la Rosa-Fox, L. Esquivias, and J. Zarzycki, Diffuss. Def. Data **53-54,** 363 (1987).
23. J.D. Mckenzie, J. Sol-Gel Sci. Technol. **2,** 81 (1994).
24. K. Morita, Y. Hu, and J. Mackenzie, J. Sol-Gel Sci. Technol. **3,** 109 (1994).
25. S. Brunauer, P.H. Emmet, and E. Teller, J. Am. Chem. Soc. **60,** 309 (1938).
26. G. Horvath and K. Kawazoe, J. Chem. Eng. Jpn. **16,** 470 (1983).
27. C. Ricolleau, M. Gandais, T. Gacoin, and J.P. Boilot, J. Cryst. Growth **166,** 769 (1996).
28. T. Schneider, M. Haase, A. Kornowski, S. Naused, and H. Weller, Ber. Bunsen-Ges. Phys. Chem. **101,** 1654 (1997).
29. AI.L. Efros and A.L. Efros, Sov. Phys. Semicond. **16,** 772 (1982).
30. Y. Wang, A. Suna, W. Mahler, and R. Kasowski, J. Chem. Phys. **87,** 7315 (1987).
31. M. Nogami, K. Nagasaka, and K. Kotani, J. Non-Cryst. Solids **126,** 87 (1992).
32. R. Thielsh, T. Böhme, R. Reiche, D. Shläfer, H-D. Bauer, and H. Böttcher, Nanostruct. Mater. **10,** 131 (1998).